45TH TURBOMACHINERY & 32ND PUMP SYMPOSIA
HOUSTON, TEXAS | SEPTEMBER 12 – 15, 2016
GEORGE R. BROWN CONVENTION CENTER

The Influence of Impeller Wear Ring Geometry on Suction Performance

Thomas Liebner
Hydraulic Engineer
ITT Goulds Pumps
Seneca Falls, NY, USA

David Cowan
Senior Hydraulic Engineer
ITT Goulds Pumps
Seneca Falls, NY, USA

Simon Bradshaw
Director of API Product Development & Technology
ITT Goulds Pumps
Seneca Falls, NY, USA

Thomas Liebner is a Hydraulics Engineer with ITT Goulds Pumps responsible for applied research and hydraulic design of engineered API process pumps. His responsibilities include – new product design, computational modeling, and hydraulic analysis for performance prediction.

Dr. Liebner has a B.S. in Mechanical and Aerospace Eng. from SUNY at Buffalo. He completed his studies for his doctorate in Mechanical Engineering at Penn State University where he performed experimental and computational modeling of particle adhesion and their liberation and entrainment in air jets.

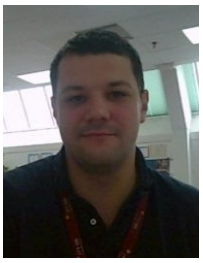

David Cowan is a Senior Hydraulics Engineer with ITT Goulds Pumps responsible for applied research and hydraulic design of engineered API process pumps. His responsibilities include the development and analysis of new and existing hydraulic products through traditional and computational methods. He is also jointly responsible for continuous development of the computational fluid dynamic analysis techniques. Prior to joining ITT Goulds, he worked as a Hydraulic Engineer for ClydeUnion Pumps.

Mr. Cowan has a B.Sc. in Aeronautical Engineering from the University of Glasgow.

Simon Bradshaw is the Director of API Product Development & Technology for ITT Goulds Pumps, in Seneca Falls NY. His responsibilities include the design and development of new products and processes. Prior to joining ITT Goulds, he worked for both Sulzer Pumps and Weir Pumps, where he held various positions of engineering and contractual responsibility. Additionally he has supported the Hydraulic Institute in the development of pump standards and best practice guides.

Mr. Bradshaw has a BEng (Hons) degree (Mechanical Engineering) from Heriot Watt University. He is a registered Chartered Engineer in the UK and a member of the Institute of Engineering Designers.

ABSTRACT

Wear rings are a necessary feature of an enclosed centrifugal impeller design. The purpose of the wear ring is to limit the leakage of fluid from the high pressure zone at the impeller outlet to the low pressure region at the impeller inlet. Several different wear ring geometries may be employed for this purpose. The choice of which geometry is utilized depends on which of the following goals are ranked most important:

- Pump efficiency
- Rotor dynamic coefficients: stiffness and damping
- Preventing contact during thermal or suction transients
- Resistance to wear from abrasive particles
- Allow later adjustment to recover original clearances as the pump wears

There have been many papers published on the effect of wear ring geometry on leakage, efficiency and rotor dynamic coefficients. However little is known about how specific wear ring geometries affect the suction performance of an impeller.

This paper seeks to examine several different wear ring geometries in common use. It will then quantify how each of these geometries affects the suction performance of the impeller over the full design flow range.

To facilitate this examination a test pump will be utilized with modular impeller eye side wear ring geometry. The physical testing will be accompanied by CFD simulations and the results will be compared.

INTRODUCTION

The primary task of a wear ring is the restriction of leakage flowrate between the rotating impeller and a stationary casing. Other secondary considerations include cost/manufacturability, wear resistance, serviceability and (for multistage pumps), rotordynamic coefficients for stiffness and damping. The effect of the wear ring on suction performance, specifically the pump NPSHr is seldom considered and at time of writing the authors are not aware of any comprehensive peer reviewed papers specifically studying the effect.

Such information as does exist tends to be limited in completeness and scope. [Lobanoff, V.S., Ross, R.R., 1992], [Henshaw, T., 2009], [Jiegang, M., et al., 2010] and [Budris, A. R., 2011], all report increases in NPSHr due to increased clearances. However gaps in information regarding the pump configuration(s) and design(s) used to derive the information, make it very difficult to determine what context to place it in.

This paper seeks to begin to fill this gap in knowledge with some initial investigations into the subject. Due to time and resource constraints it is not intended to comprehensively cover all possible permutations of the topic, but to address the effects of common design variations on suction performance. Further testing will undoubtedly be required and it is the author's intention to continue to explore the effect of additional wear ring geometries in a future paper.

TEST PUMP SETUP

The test pump selected is a 4x6-11 (100x150-280) in a single stage overhung configuration with centerline mount (OH2). In terms of overall construction it is unremarkable though consistent with the current best practice for a full compliant API 610 OH2 design.

The characteristics of the test pump are tabled below:

Parameter	Value
Running Speed	3560 RPM
BEP Head	450 ft (137 m)
BEP Flow	1670 USGPM (380m3/h)
BEP power @ 1.0 SG	232 HP (173 kW)
Specific Speed Ns (nq)	1489 (28.8)

Table 1: Test Pump Specifications

The pump was installed in a standard testing station in the large hot water tank (LHWT) test loop of company's R&D facility. The test setup complied with HI 14.6 test standards. **Figure 1** shows the test pump as installed in the test loop. Note the utilization of a removable suction casing flange and clear inlet pipe. The purpose of the removable suction casing flange was to allow more rapid changeover of different wear ring geometries. The clear inlet pipe was to allow visualization of the cavitation and recirculation flow (not part of this specific paper).

Figure 1: Pump installed in the test loop

SPECIFIC TEST PUMP DESIGN ADAPTATION

The test pump was adapted from a standard OH2 design in order to allow fitment of different wear ring geometries. **Figure 2** shows a cross-sectional view of a standard OH2 pump. .

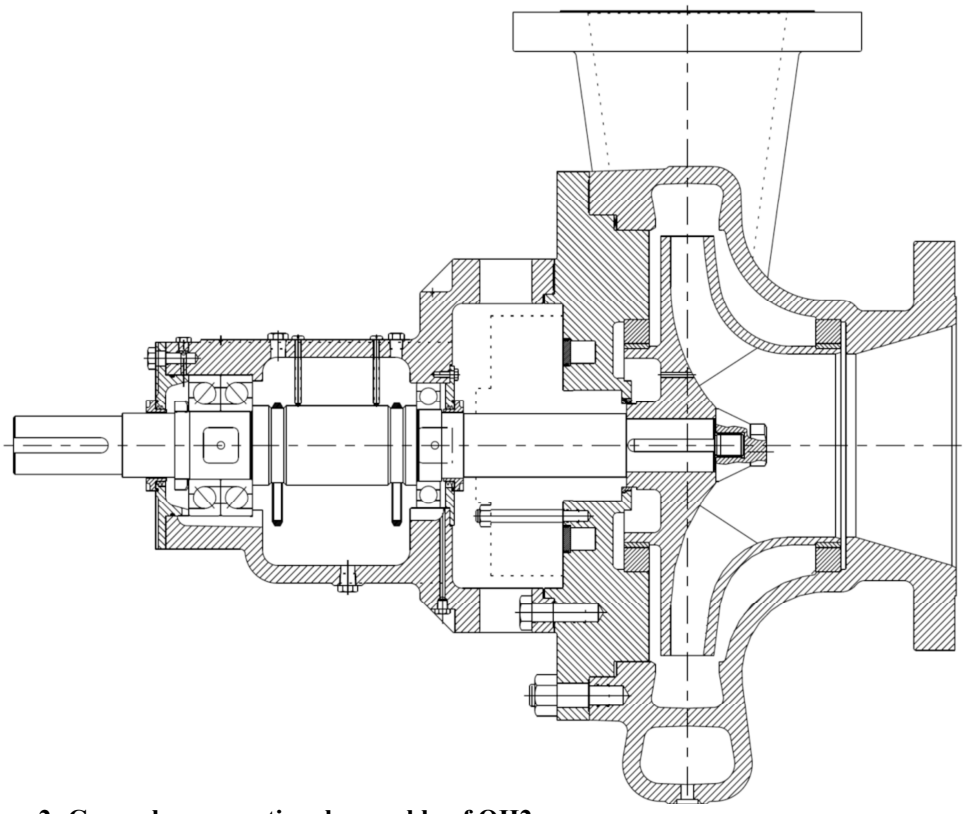

Figure 2: General cross-sectional assembly of OH2

WEAR RING DESIGN

For the test rig, three different wear ring geometries were utilized. Details of the key geometry information are tabled below.

Rings "A" and "B" shared similar geometry, the only difference being that Ring "A" had a smaller axial clearance than Ring "B". The purpose of this was to examine the effect of higher velocity radial jetting on the suction performance. Refer to **Figure 3a** for details of the design.

Ring "C" had a 45° relief in place of the axial clearance utilized in rings "A" and "B". The purpose of this was to evaluate the effect of allowing the leakage flow to diffuse and disperse into the incoming suction flow. Refer to **Figure 3b** for details of the design.

Configuration	Diametrical clearances			Axial clearance
	Company STD (75% of API 610 clearances)	API 610	2x API 610	
Ring "A"	0.014"(0.36 mm)	0.019"(0.48 mm)	0.038"(0.97 mm)	0.055"(1.4 mm)
Ring "B"	0.014"(0.36 mm)	0.019"(0.48 mm)	0.038"(0.97 mm)	0.275"(6.99mm)
Ring "C"	0.014"(0.36 mm)	0.019"(0.48 mm)	0.038"(0.97 mm)	N/A

Table 2a: Wear Ring configurations for Nss = 9568 Impeller

Configuration	Diametrical clearances			Axial clearance
	Company STD (75% of API 610 clearances)	API 610	2x API 610	
Ring "A"	0.014"(0.36 mm)	0.019"(0.48 mm)	0.038"(0.97 mm)	0.088"(2.24 mm)
Ring "B"	0.014"(0.36 mm)	0.019"(0.48 mm)	0.038"(0.97 mm)	0.257"(6.53mm)
Ring "C"	0.014"(0.36 mm)	0.019"(0.48 mm)	0.038"(0.97 mm)	N/A

Table 2b: Wear Ring configurations for Nss = 17372 Impeller

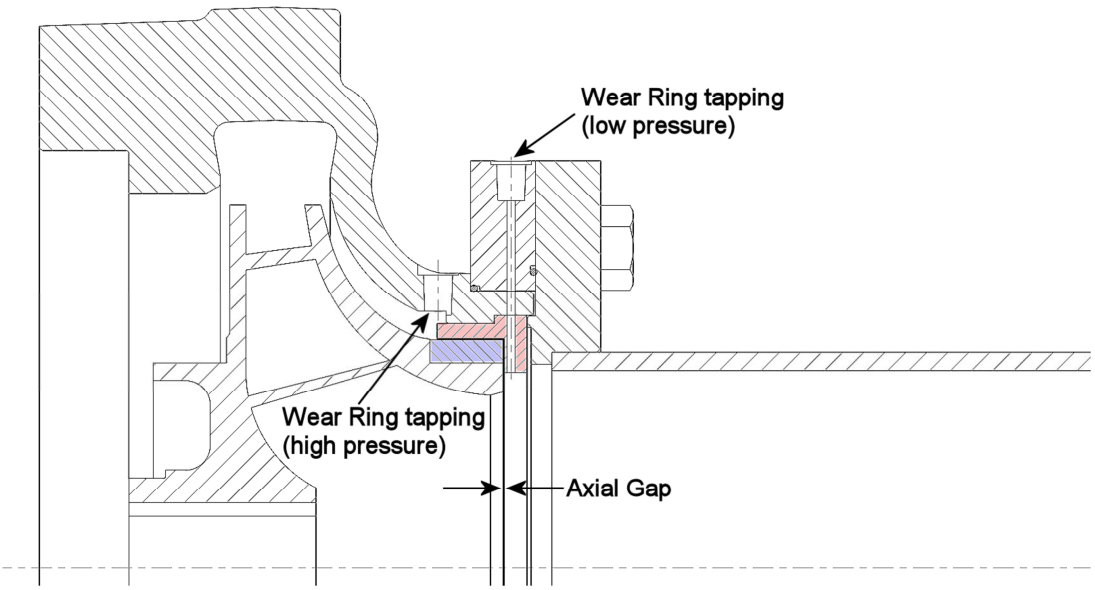

Figure 3a: Partial cross-sectional arrangement of test pump with Ring "A" and "B" configuration

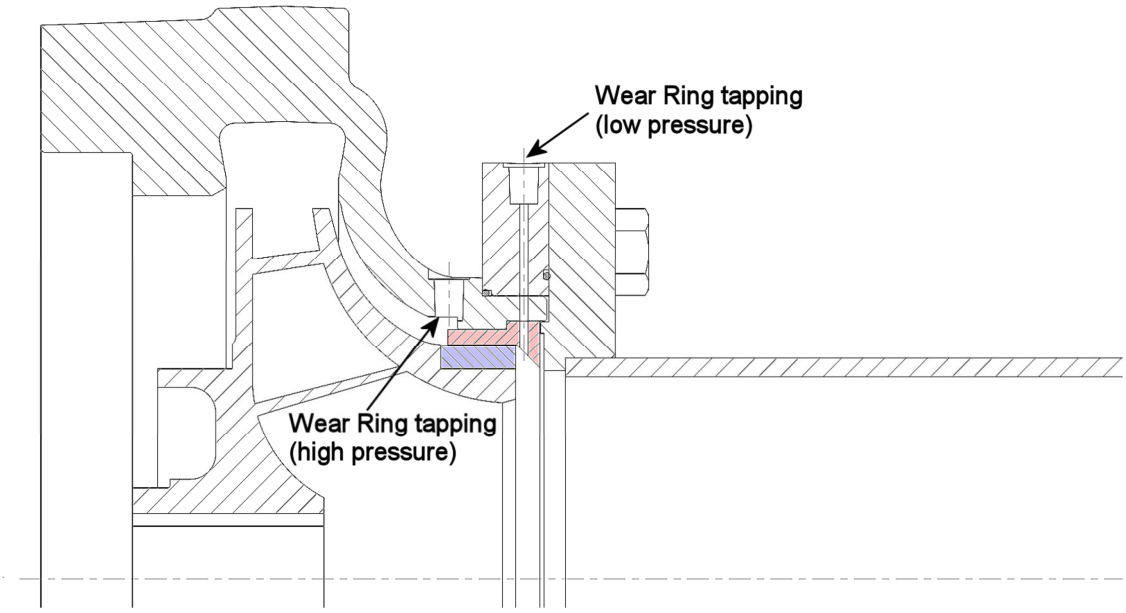

Figure 3b: Partial cross-sectional arrangement of test pump with Ring "C" configuration

IMPELLER DESIGN

For the test rig, two single entry end-suction impellers were utilized. Details of the key geometry information are tabled below. The impellers were selected in order to provide insight into the effect of wear ring leakage on both a conservative impeller design (Nss = 9568) and a more aggressive impeller design (Nss = 17372), that significantly exceeds the industry expectations and also exceeds the author's company **SgST** design guidelines for suction impellers [Bradshaw et al. 2013]. The wear ring diameter and geometries were identical for both impellers to reduce some of the testing variability.

	Impeller 1	Impeller 2
Tested Nss (S)	9568 (185)	17372 (336)
D_2 Impeller outlet diameter (in)	11	11
B_2 Impeller outlet width (in)	1	0.9
β_2 Impeller vane angle @ outlet (deg)	24	26.3
D_1 Impeller inlet eye diameter (in)	4.9	5.3
Diameter of Wear Ring (in)	7.0	7.0
β_{1t} Impeller vane angle @ inlet (deg)	29	13.2
D_1 / D_2 Impeller inlet / impeller outlet dia.	0.44	0.48

Table 3: Basic dimensions for the impellers

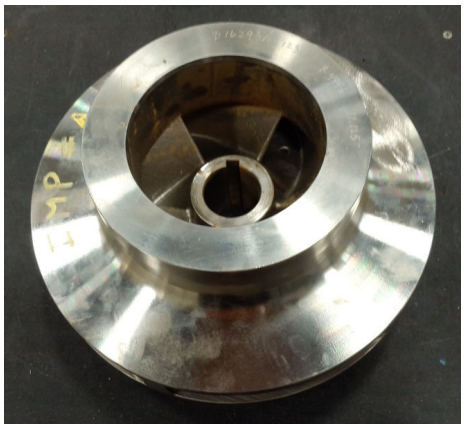

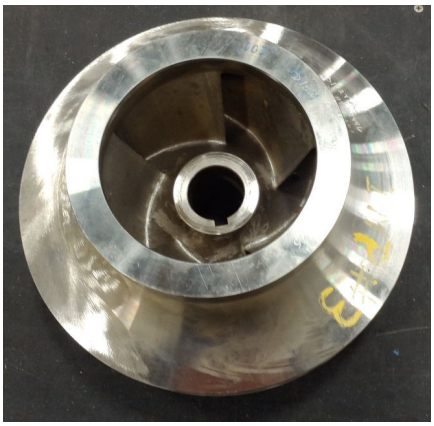

Figure 4a Nss=9568 (185) Impeller 1 **Figure 4b Nss = 17372 (336) Impeller 2**

COMPUTATIONAL FLUID DYNAMICS (CFD)

To verify the hydraulic design and testing, a computational study, conducted within the framework of the ANSYS-CFX solver, [ANSYS CFX-16.2, 2015], was undertaken. CFD was initially run as a passage analysis for each of the impellers to validate the effectiveness of a passage model in predicting the suction performance [Bradshaw et al. 2013]. In this study, further refinement of the computational method was introduced by considering a full pump assembly model. In this model, the full impeller was considered along with the volute, the front shroud, and the front wear ring clearance. This can reduce errors inherent in approximating the leakage flow which can be estimated using Yamada's methodology utilizing the differential pressure across the wear rings [Yamada, Y., 1962]. This technique is intended to be used to validate current best practices for predicting leakage rates. Additionally, the full simulation of the wear rings also has the potential to more accurately simulate the effect of leakage flow in disturbing the idealized inlet streamlines. Note that because of limited computer wall time; only Impeller 2 with the "B" Ring configuration was modeled across a range of clearances and flow rates.

For simplicity, a steady-state flow condition was utilized for this analysis. This has certain limitations as it neglects the unsteady characteristics including blade pass and system response but significantly reduces the wall time for analysis.

MESH STRUCTURE

An unstructured mesh with tetrahedral mesh elements was generated using the Simmetrix grid generation software [Simmetrix MeshSim, 2014]. A boundary layer mesh with hexahedral mesh elements was placed on wall surfaces. A minimum Δy was established such that the average y+ value on the vane surface was between 10-20. The small gap for the ring clearance provided some difficulty in producing a repeatable mesh with acceptable convergence. The standard ring clearance option provided for a radial gap of only $7x10^{-3}$ (in). The model tolerance for dimensional accuracy was limited to around $3x10^{-4}$ (in). This meant that within the clearance gap, it became difficult to accurately reproduce even 5 boundary layers on each wall surface successfully. As the tested NPSH performance for Company Standard (75% of API 610) and API 610 clearances proved to be very similar, it was decided that a

CFD simulation of only the API clearance and 2xAPI clearance would be performed. The *k-ω* model with the shear stress transport (SST) adaptation is utilized to model the turbulence and near-wall structures. For this turbulence model, a y+ of less than 30 has produced repeatable results while sufficiently capturing the near-wall characteristics. The global size was chosen as 0.006x the maximum length of the passage. The full assembly mesh was about 3 million nodes with full convergence after around 600 iterations at a compute time of 3 hours.

A grid refinement study was performed for one of the design cases to ensure that the mesh was properly constructed and would produce results of sufficient accuracy. Three meshes of increasing refinement were utilized with particular emphasis on the mesh count within the front clearance region. The results of this sensitivity study are described in **Table 4**.

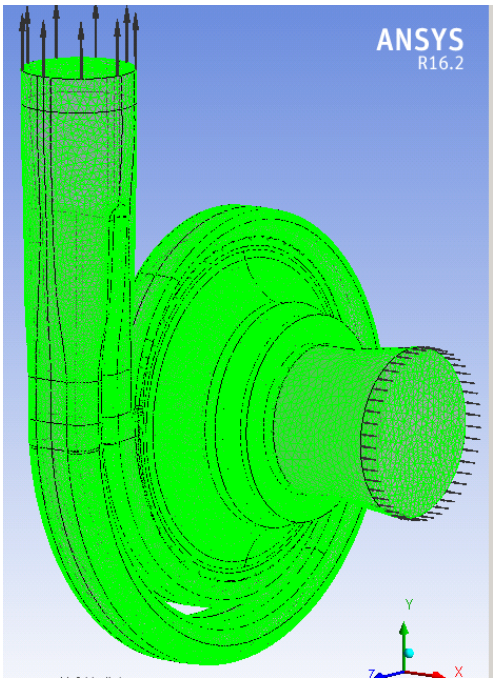

Figure 5: Sample mesh used during computational study.

As described in the book [Johann Güilich, 2010, Centrifugal Pumps 2nd Edition], approximating a grid independent solution (H_{nu}), the discretization errors (e_h) and the order (p) of the solution can be calculated utilizing solutions of grid sizes that differ by a factor of 2. The equations are listed below.

$$p \approx \frac{1}{log2} log\left(\frac{H_h - H_{4h}}{H_h - H_{2h}}\right)$$

$$e_h = \frac{H_h - H_{2h}}{2^p - 1}$$

$$H_{nu} \approx H_h + \frac{H_h - H_{2h}}{2^p - 1}$$

Total Nodes	Nodes in Sidewall	TDH [ft]	Power [HP]	Efficiency	NPSHr [ft]
2,983,802	994,802	439.6	230.1	82.7%	17.6
3,644,000	1,655,000	443.3	226	84.9%	16.8
4,789,000	2,800,000	443.5	226.3	84.9%	16.6
	p	-4.21	-3.66		-2
	e_h	3.9	-4.1	N/A	-1
	Value at $_{nu}$	443.5	226.0	N/A	16.5

Table 4: Mesh refinement sensitivity study

CFD SOLVER CRITERIA

An analysis of Impeller 2, Nss 17372, at Company Standard (75% of API 610), API 610, and 2x API 610 clearances was performed utilizing the ANSYS-CFX solver. The homogeneous two-phase mixture model is employed to model cavitation. The cavitation model is based on the Rayleigh-Plesset equation with source terms for the generation and destruction (vaporization and condensation) of vapor bubbles [Bakir et al., 2004]. The model solves for two-phases, vapor phase (α_{vapor}) and liquid phase (α_{water}), at each control volume location, with the sum of both phases equal to one ($\alpha_{vapor}+\alpha_{water}=1$) at each location. The basic assumption of the model is that all phases share the same velocity and a mixture equation is solved for the conservation of momentum. High resolution fluxes are chosen for the discretization of mean flow and turbulence equations.

As noted, the entire hydraulic passages for the full pump stage was simulated including geometry for the full impeller, the casing volute, and the front sidewall gap between the casing and impeller including the wear ring clearance as shown in **Figure 6**. For the analysis, no slip boundary conditions are applied at all wall surfaces; total pressure is specified at the inlet with the volume fraction of water as 1.0 and vapor as 0.0; mass flow rate is specified at the volute outlet.

Convergence for the velocity and momentum residuals was determined below an RMS value of 10^{-4} and occurred within 200 to 400 iterations. However, each of the computational runs required between 600 and 800 iterations to achieve full convergence of the pressure and power solutions.

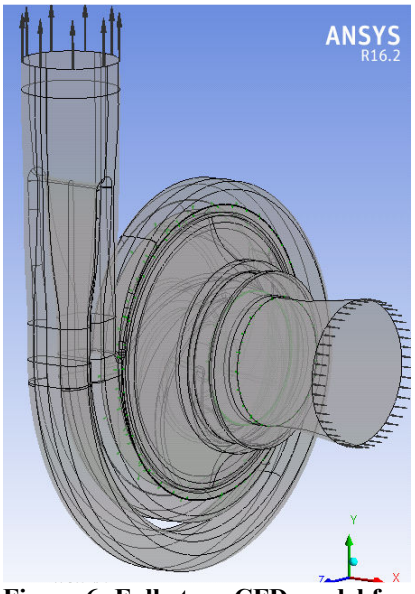

Figure 6: Full-stage CFD model for analysis

Multiple design point studies were conducted across the operating range of the Impeller 2 pump system. At each flow rate, the inlet total pressure was chosen well above the known NPSH 3% break point and the total head, power and leakage rate across the shroud ring were calculated. The simulation was repeated while gradually reducing the inlet total pressure effectively reproducing a typical NPSH test run. **Figure 7** demonstrates a typical head drop curve predicted by the computational analysis. **Figure 8** illustrates the typical streamline path for the fluid and **Figure 9** shows the NPSH 3% break points as predicted for three different sets of ring clearances.

Thus, in order to determine a single NPSH data point, multiple run points were required at decreasing suction pressures. Therefore, this quickly becomes computationally intensive both in wall-time and in hard drive storage requirements, particularly as this is a fairly large simulation model of the full pump hydraulics including the small ring clearances.

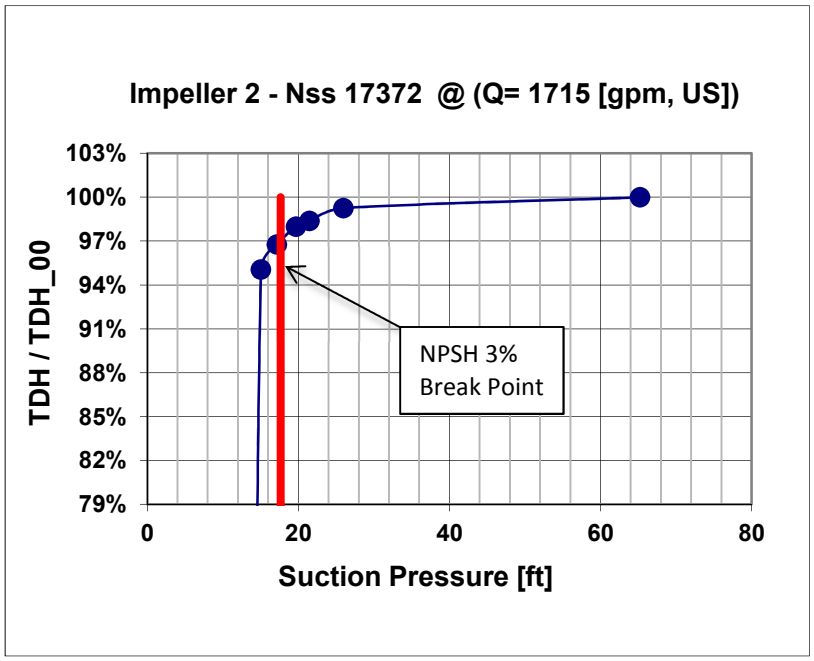

Figure 7: Typical head breakdown curve

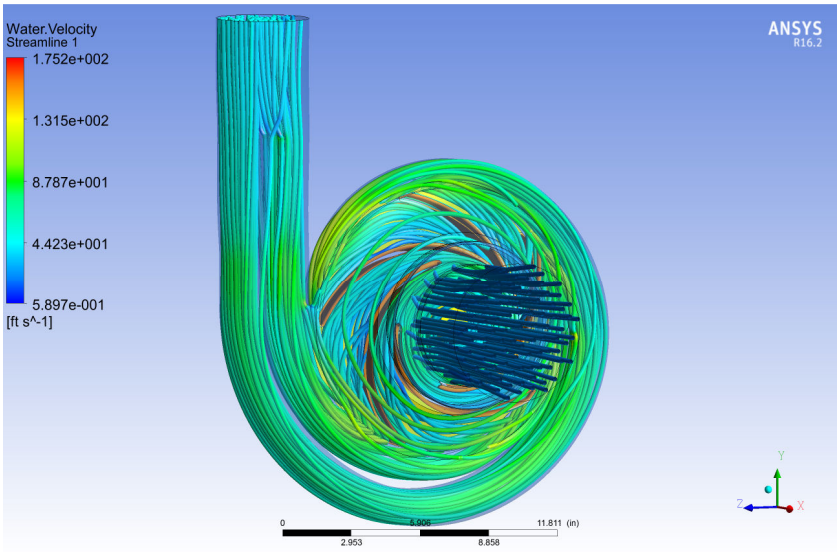

Figure 8: Streamline path representing the flow from inlet through the impeller and exiting through the dual volute.

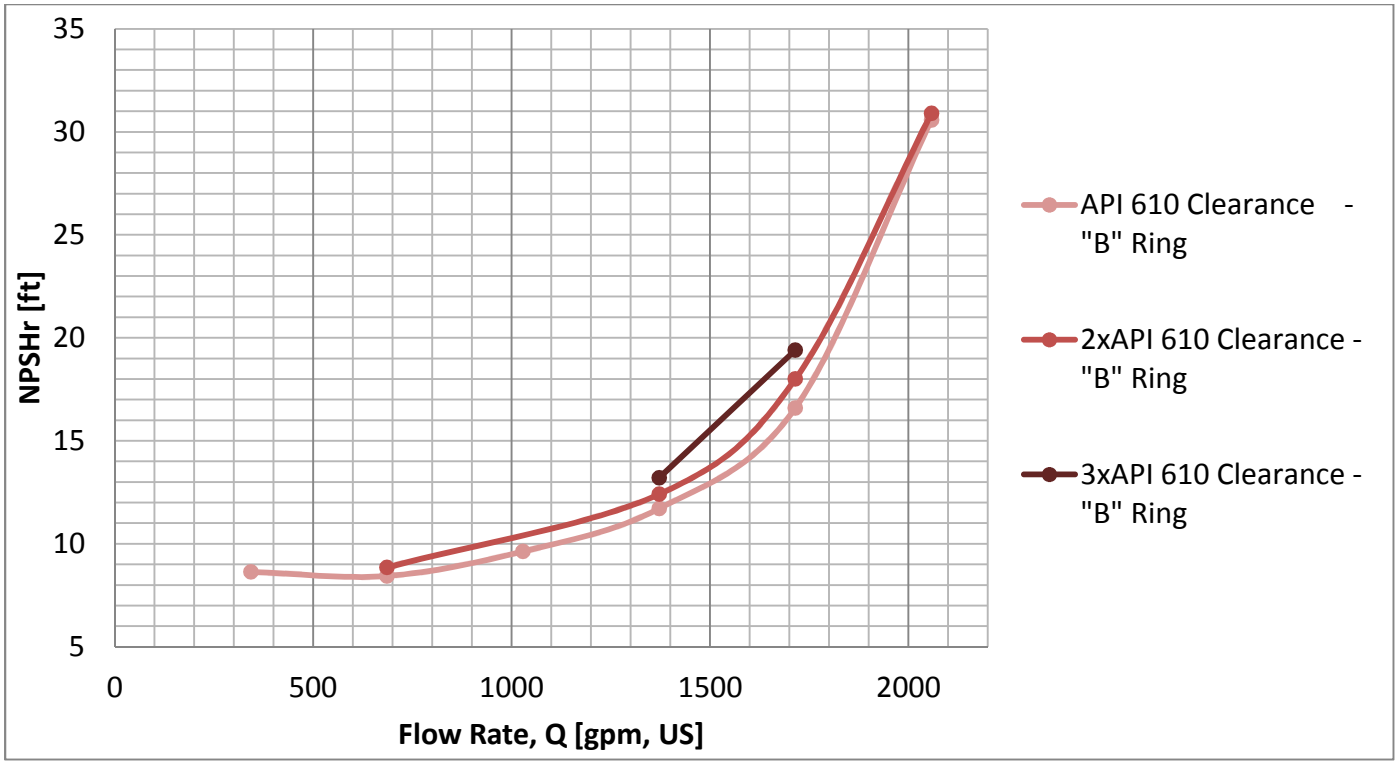

Figure 9: CFD simulation of various clearances on the front shroud ring for the Impeller 2 Nss =17372 configuration.

Note that the increase in clearances from 1xAPI 610 to 2xAPI 610 raised the predicted NPSHr by approximately 6-8%, and again by about 6-8% when going from 2xAPI 610 to 3xAPI 610 clearances.

EXPERIMENTAL RESULTS

Each impeller was subject to a full performance and NPSH test based on the criteria set out in API 610. Note that NPSHr testing typically incurs more variability than HQ testing and the expected error based on Hydraulic Institute standard 14.6 (2011) Grade 1 testing is ± 4% at low NPSHr values up to a maximum of approximately ± 1ft.

It was found that the ring geometry and axial gap had minimal effect on the NPSHr performance. **Figures 10** and **11** show a comparison at API 610 clearances of the three different ring configurations for both tested impellers. The results indicate that the tested ring geometries have minimal impact on the pump suction performance. This trend was consistent for all clearances.

In **Figure 11**, the CFD prediction was also shown. At or near BEP, the CFD under-predicts the NPSHr by about 10-15%. This can be explained based on the fact that the computer simulation considers more idealized flow conditions and cannot as easily account for actual irregularities in the surface features of the tested parts or in the inlet flow field. At flow rates much lower than BEP, near the minimum continuous sustainable flow line for the pump (MCSF), the CFD starts to over-predict the NPSHr. There are a few possible explanations for this discrepancy. First, the k-ω modeling scheme cannot accurately predict all forms of recirculation within the pump. Increased recirculation at these lower flow rates will begin to generate blockage within the impeller reducing the effective vane-to-fluid incidence angle, lowering the effective NPSHr. Additionally, the recirculation can project well into the upstream piping, which is not fully modeled within this simulation. All of these factors add to the instabilities in the fluid field caused by additional mixing and can result in poor convergence of the simulation and an unsteady solution. In this particular case, the NPSHr at off-BEP conditions is over-predicted by about 20%-30%.

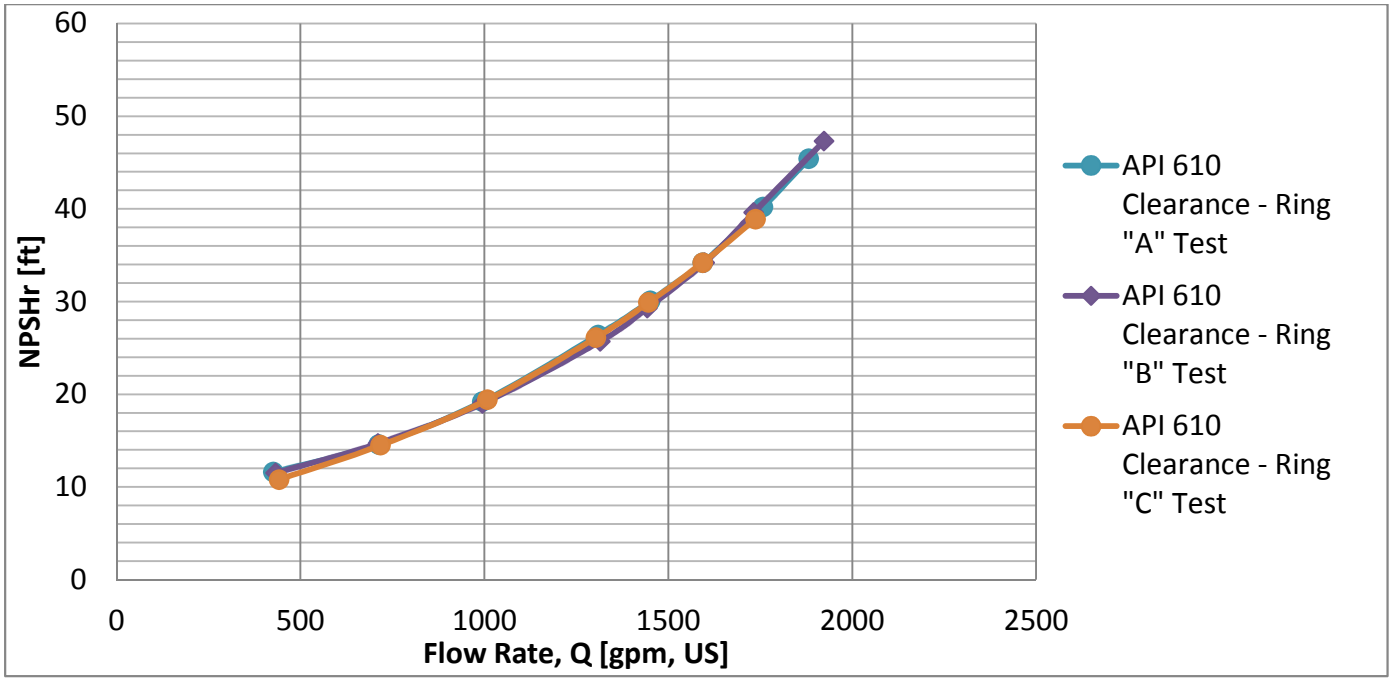

Figure 10: The varying geometry of the three ring configurations, "A", "B" and "C", as tested at API 610 clearances for Impeller 1 – Nss =9568 showing no discernible change in NPSHr performance.

Both impellers were then tested at various ring clearances, starting with Company Standard (75% of API 610), and progressing to API 610 and 2xAPI 610. **Figure 12** and **Figure 13** show a representative sample of the "B" Ring showing the increase in the suction performance as a function of the ring clearance. **Figure 13** also shows the parallel increase in CFD prediction with change in simulated ring clearance. Note that near BEP the CFD prediction is consistently under-predicting the leakage, and as the leakage path increases in size, the CFD does not show as dramatic an increase in the NPSHr prediction.

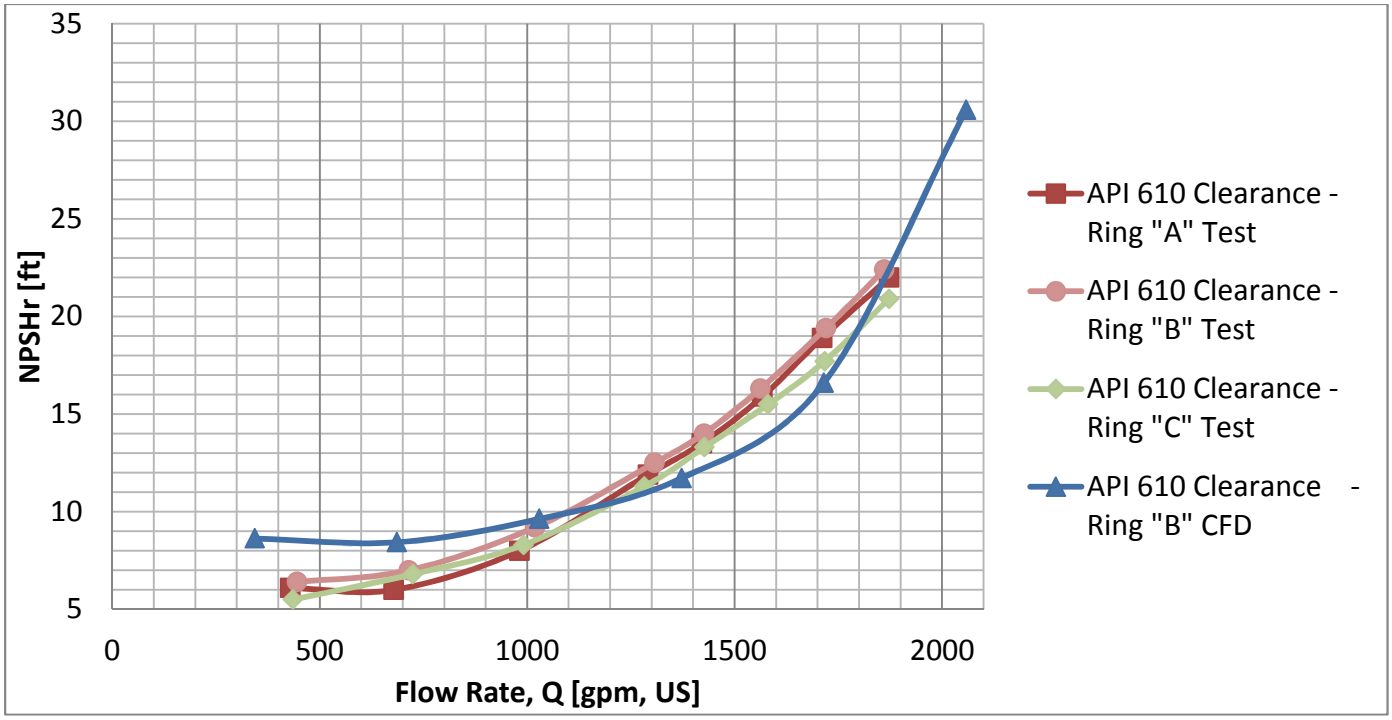

Figure 11: The varying geometry of the three ring configurations, "A", "B" and "C" for Impeller 2 – Nss= 17372, as tested at API 610 clearances showing minimal change in NPSHr performance. The results from the CFD simulation are also shown

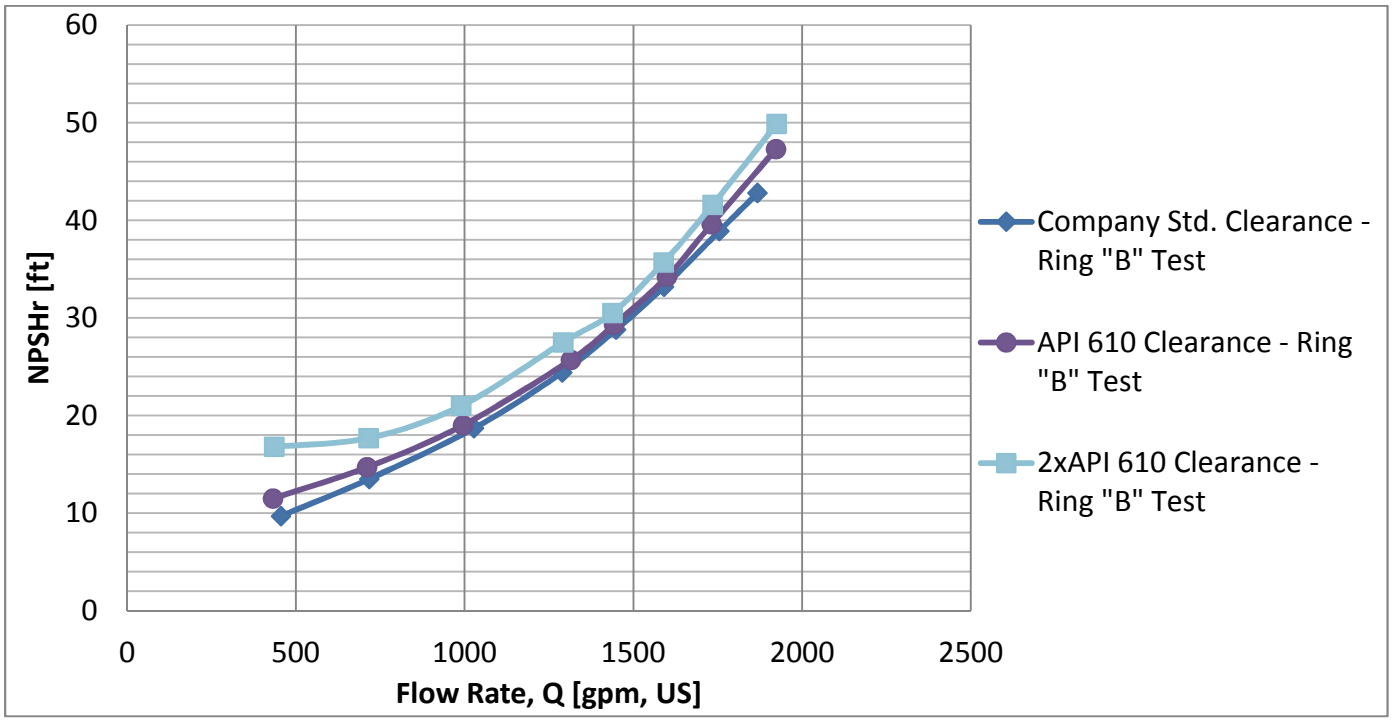

Figure 12: Test results showing variation in NPSHr curves for differing clearances for the "B" ring utilizing Impeller 1 - Nss = 9568.

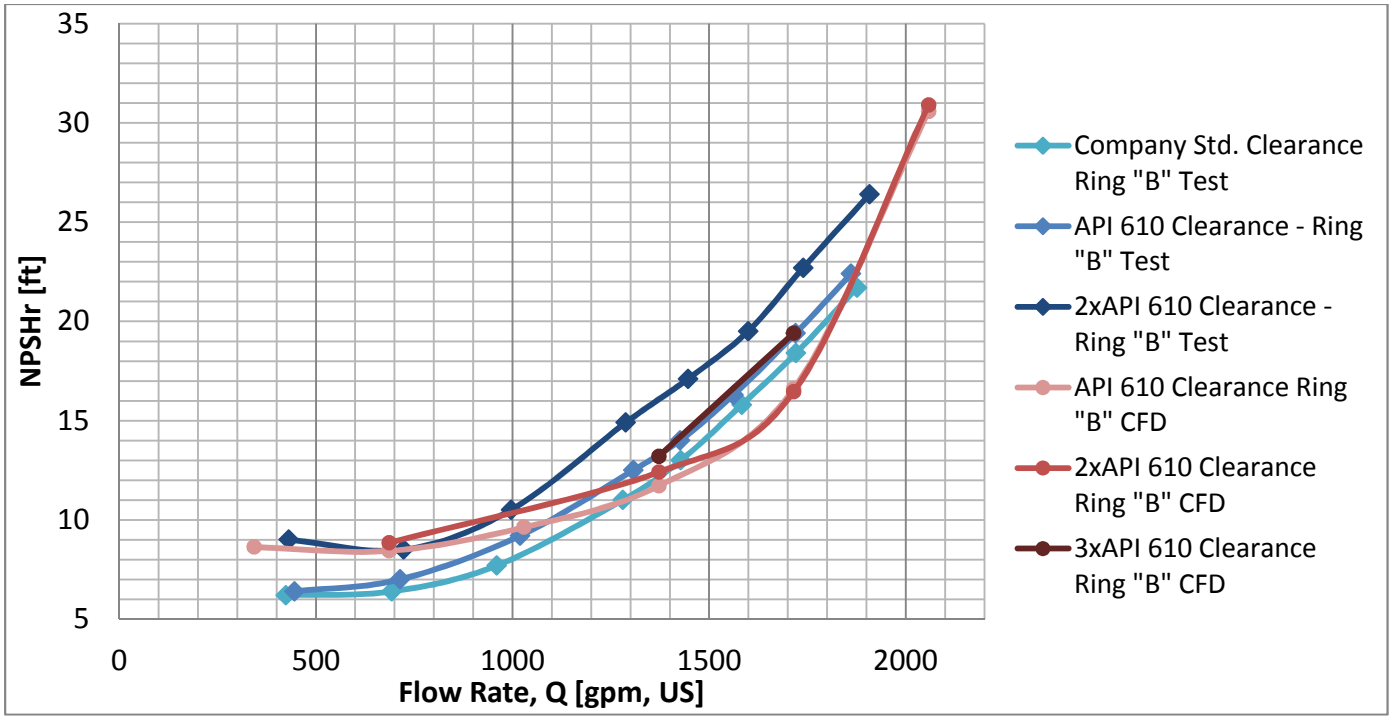

Figure 13: Test results showing variation in NPSHr curves for differing clearances for the "B" ring utilizing Impeller 2 – Nss = 17372. CFD predictions are also shown.

The tested results at the BEP point for all of the ring geometries and both impellers are summarized in **Figure 14** below. The impact of increasing the clearance on the NPSHr, both in amplitude and in percent change, was more severe for Impeller 2 – Nss = 17372 which was the more aggressive Nss impeller. In **Table 5**, the expected shift in the NPSHr curve based on increase in leakage was estimated.

For Impeller 2 – Nss = 17372, the NPSHr should increase from API 610 to 2xAPI 610 clearances based on a shift in flow equal to the leakage rate as the impeller is effectively operating at a higher flow rate than the casing. **Table 5** predicts this flow shift to be between 60-80 USGPM across the entire operating range for the pump.

However, as shown later in **Figure 15**, the actual increase in NPSHr is greater than a simple flow shift for the NPSHr curve which indicates that the increased leakage also has a negative impact on the uniformity of the flow into the suction. As the leakage flow is nearly perpendicular to the inlet flow, this can adversely impact the fluid inlet angle, particularly on the shroud side of the impeller, and can add mixing and turbulence which can exacerbate cavitation within the impeller inlet.

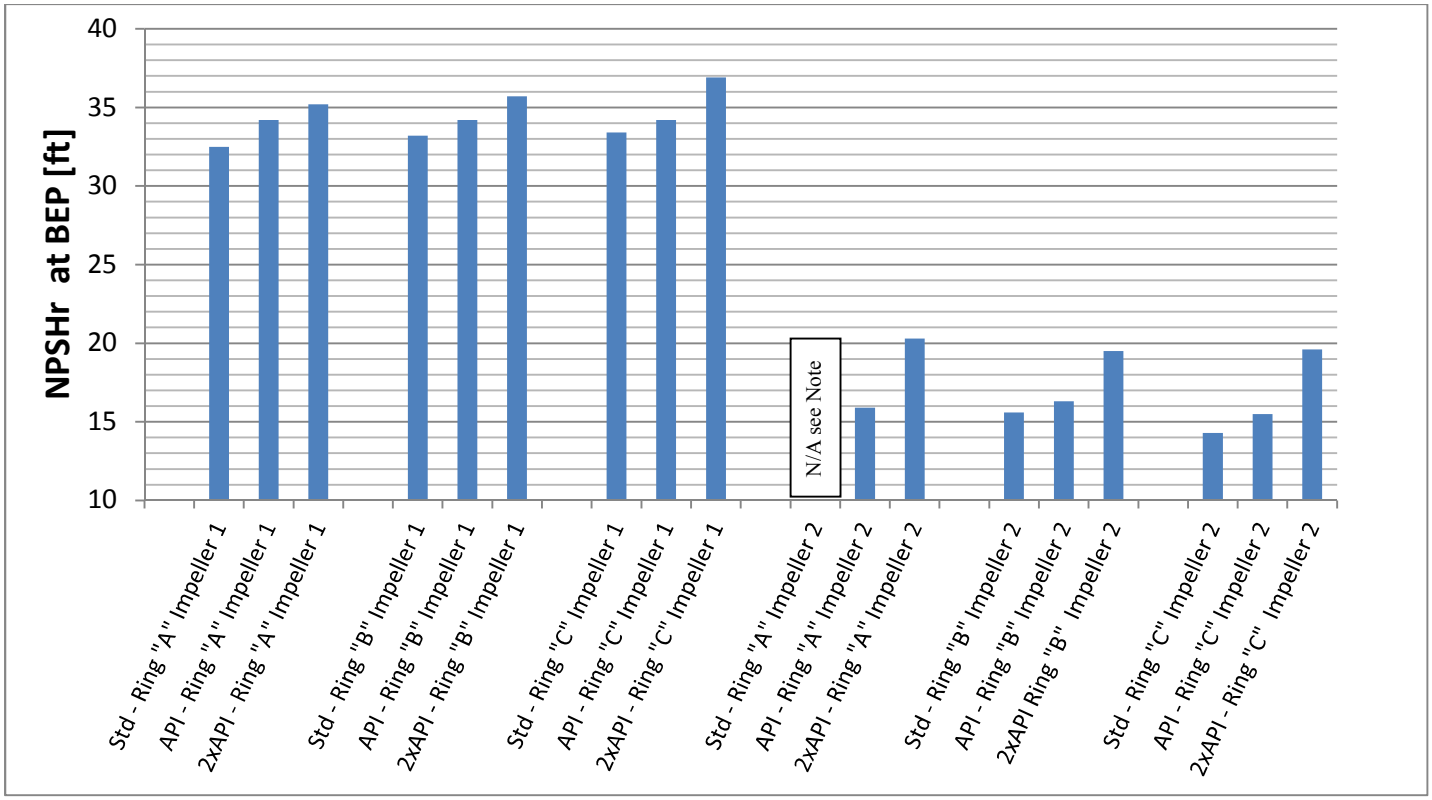

Figure 14: Summary of the NPSHr test results at the pump best efficiency point (BEP). (*Note that the test for Impeller 2 with Company Standard Clearances Ring "A", was not run due to the existing clearances for Ring "A" already being at API 610 values.)*

DISCUSSION

The CFD simulation as presented here showed some limitations in accuracy. As has been shown previously in the single passage simulation, the CFD simulation tends to under-predict the tested NPSHr at BEP [Bradshaw et al., 2013]. Discrepancies in the actual surface finish and modeled geometry, unsteady flow characteristics, and modeling simplifications can account for this discrepancy. Additionally, this particular model required very tight clearances across the wear surfaces which can be particularly difficult to model as the mesh must go from large global mesh elements to much smaller and very thin boundary layers across the ring clearance. Because of these difficulties and flow instabilities at off-BEP conditions, the reliability of NPSH results at the off-BEP conditions did not directly correlate with what was seen on test. This could potentially have been affected by inaccuracies in how the cavitation bubble is formed in the simulation and how that modifies the effective fluid incidence angle.

Additionally, as the clearance increased from 1x API 610 to 2x API 610 clearances, even when simulating near BEP, the simulation began to more severely under-predict the actual NPSHr as tested for the pump. The leakage flow generates a flow perpendicular to the bulk inlet flow into the impeller. It is probable that the mixing characteristics and the impact of this non-favorable fluid direction are being under-predicted. In fact, the leakage rate across these rings as predicted by the CFD simulation was less than what was calculated using the method presented by [Yamada, Y., 1962]. Under prediction of the leakage by CFD ranged from 20% to 40%. This could be due to variations in machining tolerances as well as the inherent difficulty in achieving acceptable meshing schemes and resolutions in fine annular gaps.

Thus, it is important that the CFD simulations are utilized with a certain degree of caution and an appropriate correction "safety" factor be applied to these predictions. Additional meshing and setup conditions will be considered in the future to determine if other setup criteria might produce a better result with a smaller correction factor.

The tested increase in NPSHr with increased clearances cannot be explained solely by increased flow through the impeller. The NPSH curve for API 610 clearances can be taken as a baseline and then modified by the computed additional leakage flow at 2x API 610 clearances. For the purposes of computing the leakage flow, the equation according to Yamada was utilized. The result is shown in **Figure 15**. Note that the actual pressure drop across the wear ring was measured (and utilized) using the tappings in the test rig to ensure accurate computation of the leakage rates as shown in **Table 5**.

Comparing that to the test result shows that NSPHr increases significantly more than can be attributed to increased leakage alone. Only around 50% of the NPSHr increase can be explained from the increased leakage across the ring clearance. Hence, the leakage flow must be impairing the velocity profile at the impeller vane leading edge contributing to mixing losses and flow instability at the impeller inlet.

1xAPI 610 Clearances			2xAPI 610 Clearances			
Discharge Flow [gpm, US]	**Δ Pressure Across Ring [ft]**	**Yamada 1xAPI [gpm]**	**Disch. Flow [gpm, US]**	**Δ Pressure Across Ring [ft]**	**Yamada 2xAPI [gpm]**	**Lkg. "Correction" [gpm, US]**
725	293.0	51.6	435	262.0	129.5	77.9
1015	284.0	50.6	725	248.0	127.2	76.6
1305	270.0	48.5	1015	230.0	122.3	73.8
1450	266.0	48.5	1305	220.0	122.3	73.8
1595	256.0	48.1	1450	218.0	121.4	73.3
1740	247.0	47.3	1595	213.0	119.5	72.2
1885	235.0	46.3	1740	206.0	117.3	71
435	321.0	52.9	1885	196.0	112.8	59.9

Table 5: Summary of pressure measurements across the wear ring for Impeller 2 at Nss 17372 with the estimation of the leakage rates for the API 610 and 2xAPI 610 clearances.

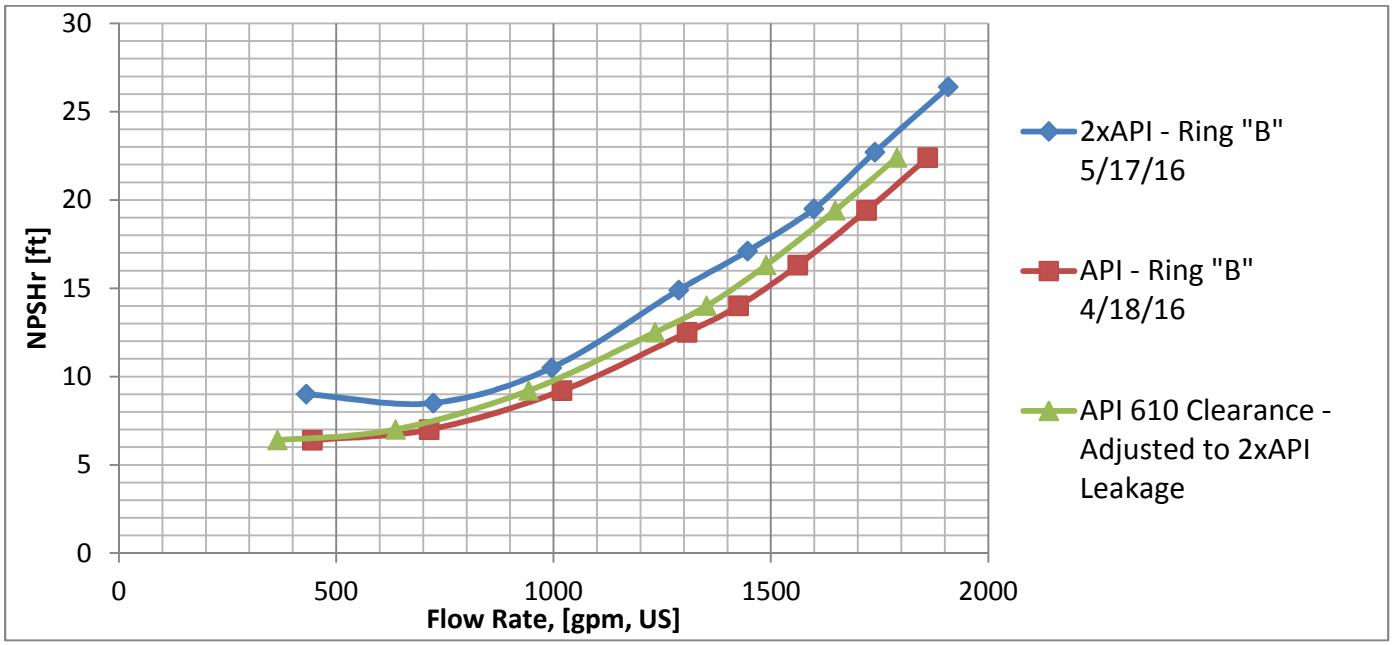

Figure 15: A comparison of the API 610 clearance test and 2xAPI clearance test and an adjusted estimate of performance assuming that the change in leakage rate is the only influence on the shift in NPSH between the two tests.

The tested performance for the three different wear ring geometries, "A", "B" and "C" showed very little variation in curve shape and no quantifiable trend of changes to NPSHr performance. Pressure measurements were taken at the high and low pressure sides of the ring clearance. There were no noticeable pressure differences between the three ring geometries. This indicates that the leakage rate across the ring for these three geometries is essentially equal. Also, jetting and mixing effects are comparable regardless of the axial gap tested. This supports the conclusion that in the case of small radial clearances which are the primary mode of determining leakage rates, and changes in the axial gap between the impeller and casing will have minimal impact on the NPSH performance. This conclusion should be used with caution for pumps of other specific speeds than as tested here or for axial gaps smaller than the range explored during testing.

A few additional conclusions can be drawn. The test results show that above a certain wear ring clearance, a large change in NPSHr can be observed. This was particularly significant for Impeller 2 – Nss = 17372 with an aggressive suction performance. From the test results at the impeller BEP, NPSHr was increased by only 3% and 4%, 1ft and 0.7ft, respectively for the two impellers when the wear ring clearance was increased from Company Standard to API 610. However, the NPSHr was increased an additional 5% and 21%, 1.5ft and 3.2ft, respectively for the two impellers when the wear ring clearance was increased from API 610 to 2x API 610. The relevant NPSH increases are tabled below in **Table 6**. The finding is important because the normal "End of Life" guidance provided by most pump manufacturers is that the pump should be taken out of service and repaired when the wear ring clearances reach 2x the original "As New" values.

Configuration with the Ring "B"	Impeller 1 – Nss 9568 NPSHr @ BEP [ft]	Impeller 1 – Nss 9568 change over baseline	Impeller 2 – Nss 17372 NPSHr @ BEP [ft]	Impeller 2 – Nss 17372 change over baseline
Company STD (75% of API 610 clearances)	33.2	N/A	15.6	N/A
API 610	34.2	1.03	16.3	1.04
2x API 610	35.7	1.08	19.5	1.25

Table 6: NPSHr increase over baseline for Impeller 1 and Impeller 2

Hydraulic Institute Standard 9.6.1 (2012) provided recommendations for NPSH margin for a variety of different services and is widely utilized. *A review of this standard returns the result that of 17 services for which the standard provides NPSH margin guidelines, 15 services had a recommended NPSH margin of 1.1 or less in the POR*. One important consequence is that even excluding other effects, at "End of Life" clearances, pumps in the services listed in HI 9.6.1 (2012) may be operating at or below NPSHr resulting in the pump having signficant head impairment, efficiency impairement,increased vibration, and hence the potential for machine degradation and failure.

The increase in vibration is particularly significant since there is a strong correlation between the level of vibration and a reduction in the MTBF. For example ISO 10816-7 (2009) defines bands for vibration levels in centrifugal pumps. These bands are A, B, C and D with A being "Excellent" and D being "Bad – damage causing". For the 232 HP (173 kW) pump with a rigid foundation, the vibration only has to increase from 0.11 in/s RMS (2.8 mm/s) to > 0.18 in/s RMS (4.5 mm/s) for the pump to have gone from unlimited long term operation to damaging vibration. Such a threshold is easy to cross if the pump is operated with no NPSH margin (i.e 3% head breakdown) and hence extensive cavitation.

HI standard 9.6.1 (2012) does not discuss the effects of wear ring degradation and increased clearance on NPSHr (and consequently NPSH margin), which given the results of the testing outlined in this paper is a significant omission.

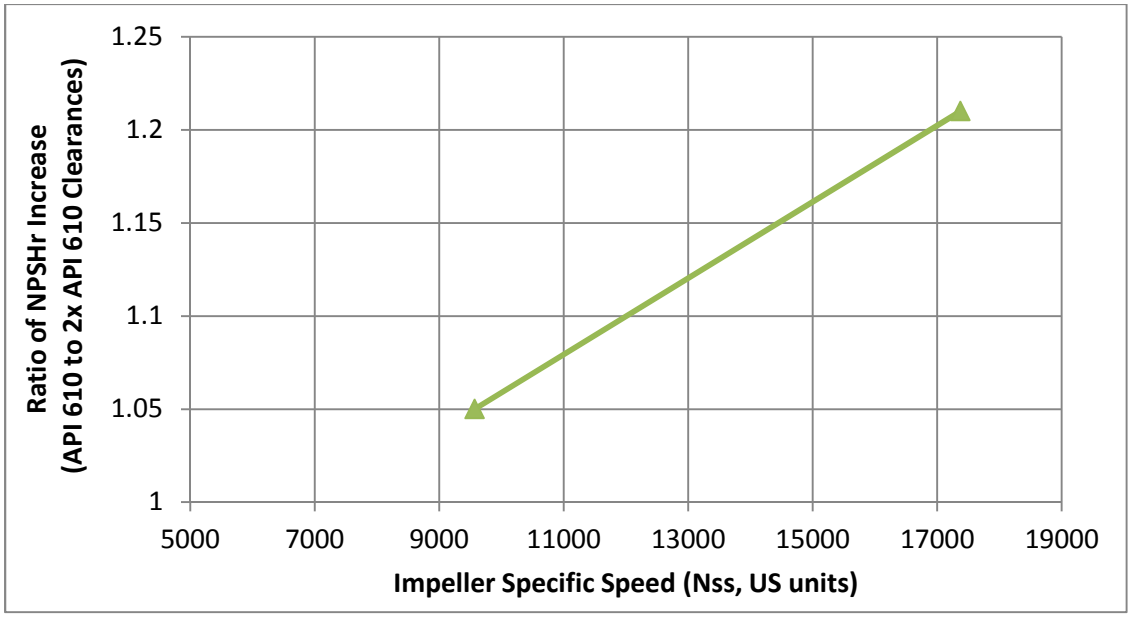

Figure 16: A comparison of the increase in NPSHr at "End of Life" to Impeller Nss

SUMMARY AND CONCLUSIONS

For any given ring geometry, the increase in NPSHr cannot be explained solely by increased wear ring leakage shifting the pump NPSH curve. The increased leakage causes degradation of the velocity profile seen at the impeller vane leading edge.

The testing results showed that for closed impellers of both a conservative and aggressive Nss design, NPSHr increased noticeably as the wear ring clearance reached "End of Life" clearances, being twice the "As New" API 610 clearances. For these impeller designs, the increase of NSPHr within the POR is the same as or more than the NPSH margin recommended by Hydraulic Institute Standard 9.6.1(2012). Consequently when the HI criteria are strictly applied, a significant population of pumps may operate with significant head impairment and loss of reliability before their "End of Life" clearances are reached.

As a minimum this should be recognized as a risk in HI Standard 9.6.1(2012) and further research should be done to better establish the change in NPSHr over a wider range of clearances including fully axial wear surfaces, open vane pump designs, and additional pump specific speeds.

NOMENCLATURE

BEP = best efficiency point (flow rate) of the pump
CFD = computational fluid dynamics
API = American petroleum institute
$NPSH_A$ = available net positive suction head
$NPSH_3$ = net positive suction head at 3% head drop
$NPSH_r$ = net positive suction head required (= $NPSH_3$)
Ns = specific speed (RPM, USGPM, ft)
Nss = suction specific speed (RPM, USGPM, ft)
S = suction specific speed (RPM, m^3/hr, m)
Q = pump flow rate USGPM (m^3/hr)

MCSF = Minimum Continuous Stable Flow
MTBF = Mean Time Between Failures
POR = Preferred Operating Region – normally in the range of 70% to 110% of BEP
D_1 = impeller eye diameter
β_1 = impeller vane inlet angle
D_2 = impeller outlet diameter
B_2 = impeller outlet width
β_2 = impeller vane outlet angle

REFERENCES

1. ANSYS-16.2 CFX Solver Theory Guide, 2015.
2. Simmetrix, Simulation Modeling Suite, MeshSim, 2014.
3. Lobanoff, V.S., Ross, R.R., 1992, *Centrifugal Pumps: design & application 2nd Edition,* Figure 8-12, Butterworth-Heinemann
4. Henshaw, T., 2009, *Effect of Internal Clearances on NPSHr*, Pumps & Systems
5. *Budris, A. R., 2011, Pump NPSHr and NPSH Margin Uncertainties*, WaterWorld
6. Jiegang, M., et al., 2010, *Effect of Clearance of Impeller Wear – rings on Cavitation Characteristic of Agriculture Pump*, Journal of Agricultural Mechanization Research, Hangzhou, China.
7. Schiavello, B., and Visser, F. C., 2008, *Pump Cavitation – Various NPSHr Criteria, NPSHa Margins, and Impeller Life Expectancy*, Proceedings of the 24th International Pump Users Symposium, 2008, Turbomachinery Laboratory, Department of Mechanical Engineering, Texas A&M University, College Station, TX.
8. Güilich, J-F., *Centrifugal Pumps, 2010, Second Edition*
9. Bradshaw, S., et al., 2013, *Influence of Impeller Suction Specific Speed on Vibration Performance*, Proceedings of the 29th International Pump Users Symposium, 2013, Turbomachinery Laboratory, Department of Mechanical Engineering, Texas A&M University, College Station, TX.
10. Yamada, Y., Resistance of Flow through an Annulus with an Inner Rotating Cylinder, Bulletin of JSME, Vol. 5 (1962), p. 302-310.

ACKNOWLEDGEMENTS

Special thanks to John Salerno (Jr.) for his help with all the necessary parts, Imtiyaz Palsaniya for his design of the test rig and Jeff Crance for all his help with the extensive testing and data logging..